Phase diagram and re-entrant fermionic entanglement in a hybrid Ising-Hubbard ladder

H. S. Sousa,[1,2] M. S. S. Pereira,[1] I. N. de Oliveira,[1] J. Strečka,[3] and M. L. Lyra[1]

[1]*Instituto de Física, Universidade Federal de Alagoas 57072-970 Maceió, Alagoas, Brazil*

[2]*Instituto Federal do Piauí, Campus Pedro II, 64255-000 Pedro II-Piauí, Brazil*

[3]*Department of Theoretical Physics and Astrophysics, Faculty of Science, P.J. Šafárik University, Park Angelinum 9, 040 01 Košice, Slovakia*

(Received 23 January 2018; revised manuscript received 23 March 2018; published 14 May 2018)

The degree of fermionic entanglement is examined in an exactly solvable Ising-Hubbard ladder, which involves interacting electrons on the ladder's rungs described by Hubbard dimers at half-filling on each rung, accounting for intrarung hopping and Coulomb terms. The coupling between neighboring Hubbard dimers is assumed to have an Ising-like nature. The ground-state phase diagram consists of four distinct regions corresponding to the saturated paramagnetic, the classical antiferromagnetic, the quantum antiferromagnetic, and the mixed classical-quantum phase. We have exactly computed the fermionic concurrence, which measures the degree of quantum entanglement between the pair of electrons on the ladder rungs. The effects of the hopping amplitude, the Coulomb term, temperature, and magnetic fields on the fermionic entanglement are explored in detail. It is shown that the fermionic concurrence displays a re-entrant behavior when quantum entanglement is being generated at moderate temperatures above the classical saturated paramagnetic ground state.

DOI: 10.1103/PhysRevE.97.052115

I. INTRODUCTION

Low-dimensional quantum spin chains have been extensively explored in the context of quantum information processing due to the possibility of creation and distribution of quantum entanglement between specific spin units acting as qubits [1–13]. The degree of entanglement can also be tuned by a local magnetic field, thus allowing a fine control of intrinsic quantum correlations. Many magnetic compounds have their relevant magnetic interactions along spin chains and ladders, the latter ones are, for instance, realized in a large family of copper oxide superconducting ceramics [14–18]. In addition, analogical structures can also be realized in arrays of coupled cavity-QED and NMR systems [19–22]. Very recently, progress has been made towards the experimental extraction of entanglement witnesses using ultracold atoms trapped in optical lattices [23,24].

Theoretical studies of quantum entanglement in low-dimensional spin chains are traditionally focused on systems composed of localized spins interacting through an antiferromagnetic Heisenberg-like exchange coupling [1,25–32]. In this case, the unsaturated nature of the sublattice magnetization of the antiferromagnetic ground state results in a very localized and relatively low degree of quantum entanglement between neighboring spins, especially for isotropic Heisenberg couplings [33–35]. Besides, thermal fluctuations and the action of an external magnetic field have been shown to degrade the bipartite entanglement, which may occasionally display re-entrant features [1].

The degree of quantum entanglement has also been investigated in hybrid spin models assuming both classical Ising as well as quantum Heisenberg exchange interactions [36–50]. The intercalation of Ising and Heisenberg couplings in spin chains is motivated by two main features. First, most of these models become exactly solvable, and they thus offer a deeper understanding of the role of thermal fluctuations and external magnetic field on the quantum entanglement between neighboring spins. Second, the absence of quantum correlations between spins separated by classical Ising couplings leads to a pronounced enhancement of the quantum entanglement between the Heisenberg-coupled spin pair in comparison with the one achieved in pure Heisenberg chains. From this perspective, hybrid classical-quantum spin models afford an interesting class of physical systems, which exhibit a high degree of quantum entanglement surviving over a wider range of temperatures and magnetic fields. To date, exact solutions have been found for several model geometries including alternating Ising-Heisenberg chains, diamond chains, ladders, and tubes [36–50].

Recently, a new class of hybrid quantum spin models being composed of localized Ising spins intercalated by mobile electrons was introduced [51,52]. A hybrid model of this type was first introduced for a diamond chain and demonstrated to display several unconventional features, such as a rich phase diagram, magnetization plateaus, multipeaked specific heat curves [51], as well as a pronounced magnetocaloric effect [52]. The fermionic quantum entanglement between a pair of intercalating electrons has also been explored in several variants of such a hybrid diamond chain [44,53–55]. In addition, we have also proposed a hybrid spin-electron ladder, which captures some features present in a family of superconducting cuprates [56].

Motivated by the recent experimental advances on the quantification of quantum entanglement in Bose-Hubbard chains [24], we will introduce a new solvable Ising-Hubbard ladder on which the degree of quantum entanglement on the ladder rungs can be analytically computed. Each ladder rung will be composed of the Hubbard dimer containing two mobile electrons, which may undergo a quantum-mechanical hopping process between the dimer sites and will be subject to an

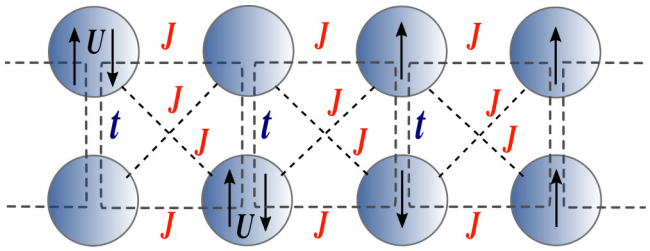

FIG. 1. A schematic of the Ising-Hubbard ladder. The ladder rungs are composed of Hubbard dimers at half-filling on each rung, which contain two mobile electrons per dimer being subject to the hopping term t and the on-site Coulomb term U. The inter-rung coupling J has an Ising-like nature.

on-site Coulomb term. The neighboring rungs will be coupled together through an Ising-like exchange coupling. We will report the exact ground-state phase diagram of the present model. The fermionic concurrence between the electrons localized in a given rung will be examined as a function of temperature and magnetic field. Particularly, we will show that thermal fluctuations can induce a quantum entanglement above a classical ground state. We will also provide a detailed analysis of the influence of hopping term, Coulomb term, temperature, and magnetic field on the degree of fermionic entanglement.

II. THE ISING-HUBBARD LADDER AND GROUND-STATE PHASE DIAGRAM

Let us consider a hybrid Ising-Hubbard ladder at half-filling on each rung (see Fig. 1). Each ladder rung is composed of a Hubbard dimer containing two mobile electrons, which undergo a quantum-mechanical hopping process between two sites of a specific dimer characterized by the hopping amplitude t. In this sense, the electrons become strictly localized when they possess the same spin state due to the validity of Pauli's exclusion principle. The electrons with opposite spins can eventually occupy the same site of a dimer and, in this case, they experience an on-site Coulomb interaction. Both cases of repulsive and attractive Coulomb interactions will be considered hereafter. Although most of the physical systems are being subject to a repulsive Coulomb term $U > 0$ due to the repulsive character of the electron-electron interaction, there may eventually appear an effective attractive Coulomb term $U < 0$ as a result of underlying interactions of the electrons with molecular vibrations or excited electronic states favoring electron-electron pairing in superconductors [57,58]. The interaction between the electrons from neighboring rungs is taken into account by an Ising-like exchange coupling J. The introduced model thus retains a quantum-mechanical interaction between two electrons from the same rung, whereas the interaction between electrons from neighboring rungs is treated classically through an Ising exchange coupling.

It is important to stress some relevant aspects of the presently introduced model. First, the Ising-like inter-rung coupling impairs a quantum entanglement between electrons from distinct rungs, at least, for magnetic fields applied along the Ising (easy) axis. Therefore, the present model can only generate quantum entanglement between electrons from the same rung. The transfer of the entangled quantum state along the chain would require some degree of inter-rung coupling between the transversal components of the spins. Despite that, it has been demonstrated that mixed Ising-Heisenberg spin ladders can accurately capture the ground-state properties of fully quantum Heisenberg ladders in the regime of weak inter-rung coupling [39,47] where the ground state is composed of rung singlets [59,60]. In this sense, the build up of intrarung entanglement can be fairly analyzed considering an Ising-like inter-rung coupling. In order to describe the dynamics of this quantum entanglement transfer, some transverse coupling would be in order. Even though quantum entanglement in the ground-state would remain strongly localized [33–35]. For example, it just appears between first neighbor spins in the ground state of an isotropic antiferromagnetic Heisenberg chain [33,34]. The study of quantum-state transfer dynamics is out of the scope of the present paper and will be left for a future contribution. As a final remark, we would like to state that, although we are not deriving the introduced model from a more fundamental microscopic model, such as a fully quantum many-body Hubbard model, several magnetic compounds have the Ising-like character of their exchange couplings due to an underlying zero-field splitting leading to a strong Ising anisotropy [61,62].

The Hamiltonian of the hybrid Ising-Hubbard ladder we are introducing has the form

$$\mathcal{H} = \sum_{i=1}^{N} \Bigg\{ J \sum_{\ell,\ell'=1}^{2} S^{z}_{\ell,i} S^{z}_{\ell',i+1} + t \sum_{\gamma=\uparrow,\downarrow} (c^{\dagger}_{1,i,\gamma} c_{2,i,\gamma} + \text{H.c.}) + U \sum_{\ell=1}^{2} (n_{\ell,i,\uparrow} n_{\ell,i,\downarrow}) - H \sum_{\ell=1}^{2} S^{z}_{\ell,i} \Bigg\}, \tag{1}$$

where $c^{\dagger}_{\ell,i,\gamma}$ and $c_{\ell,i,\gamma}$ are fermionic creation and annihilation operators for an electron with the spin $\gamma = \uparrow, \downarrow$ and $n_{\ell,i,\gamma} = c^{\dagger}_{\ell,i,\gamma} c_{\ell,i,\gamma}$ is the respective number operator. $S^{z}_{\ell,i}$ stands for the z component of the total spin operator at the dimer site $\ell = 1,2$ of the ith rung, which takes the value of $S^{z}_{\ell,i} = 0$ when the site is empty or contains two electrons with opposite spins, otherwise, it takes the values of $S^{z}_{\ell,i} = \pm 1$. The parameter J denotes the Ising-like exchange coupling between the electrons from neighboring rungs, whereas we will further focus on the most interesting case of an antiferromagnetic coupling $J > 0$. The other parameters have the following physical meaning: t is the intrarung hopping amplitude, U is the Coulomb term [$U > 0$ ($U < 0$) stands for repulsive (attractive) electron-electron interaction], and H is an external magnetic field applied along the z direction.

The Hamiltonian (1) can be exactly diagonalized due to the Ising-like nature of the inter-rung coupling J and the magnetic field H coupled to the z component of spin. We start by diagonalizing the Hubbard-like Hamiltonian of an isolated rung, which can be put in the local state basis spanned over six available electronic configurations of a single Hubbard dimer $\{|\uparrow\downarrow;0\rangle, |0;\uparrow\downarrow\rangle, |\uparrow;\downarrow\rangle, |\downarrow;\uparrow\rangle, |\uparrow;\uparrow\rangle, |\downarrow;\downarrow\rangle\}$ into the following

matrix form:

$$\mathcal{H}_i^0 = \begin{pmatrix} U & 0 & t & t & 0 & 0 \\ 0 & U & t & t & 0 & 0 \\ t & t & 0 & 0 & 0 & 0 \\ t & t & 0 & 0 & 0 & 0 \\ 0 & 0 & 0 & 0 & -2H & 0 \\ 0 & 0 & 0 & 0 & 0 & 2H \end{pmatrix}. \quad (2)$$

The eigenvalues of the dimer Hamiltonian (2) can be obtained by a straightforward diagonalization procedure,

$$\begin{aligned} \lambda_1 &= \frac{U+\sqrt{\Delta}}{2}, \\ \lambda_2 &= \frac{U-\sqrt{\Delta}}{2}, \\ \lambda_3 &= U, \\ \lambda_4 &= 0, \\ \lambda_5 &= -2H, \\ \lambda_6 &= 2H, \end{aligned}$$

whereas the respective eigenvectors are given by

$$\begin{aligned} |\lambda_1\rangle &= \frac{2t}{\sqrt{\Delta - U\sqrt{\Delta}}}[|\uparrow\downarrow;0\rangle + |0;\uparrow\downarrow\rangle - \alpha_1|\uparrow;\downarrow\rangle \\ &\quad - \alpha_1|\downarrow;\uparrow\rangle], \\ |\lambda_2\rangle &= \frac{2t}{\sqrt{\Delta + U\sqrt{\Delta}}}[|\uparrow\downarrow;0\rangle + |0;\uparrow\downarrow\rangle - \alpha_2|\uparrow;\downarrow\rangle \\ &\quad - \alpha_2|\downarrow;\uparrow\rangle], \\ |\lambda_3\rangle &= \frac{1}{\sqrt{2}}[|\uparrow\downarrow;0\rangle - |0;\uparrow\downarrow\rangle], \\ |\lambda_4\rangle &= \frac{1}{\sqrt{2}}[|\uparrow;\downarrow\rangle - |\downarrow;\uparrow\rangle], \\ |\lambda_5\rangle &= |\uparrow;\uparrow\rangle, \\ |\lambda_6\rangle &= |\downarrow;\downarrow\rangle, \end{aligned}$$

where

$$\begin{aligned} \Delta &= U^2 + 16t^2, \\ \alpha_1 &= \frac{U-\sqrt{\Delta}}{4t}, \\ \alpha_2 &= \frac{U+\sqrt{\Delta}}{4t}. \end{aligned}$$

With all dimer eigenvalues and eigenstates at hand, one can readily find all possible ground states of the Ising-Hubbard ladder. Among the ladder's states with antiparallel spins, $|\lambda_2\rangle$ has the lowest energy for all finite values of the Hubbard coupling and hopping amplitude. This rung state has no net spin along the z direction to interact with the neighboring rungs via the Ising exchange coupling or to couple with the external field. States $|\lambda_5\rangle$ and $|\lambda_6\rangle$ have a net spin. Therefore, the possible ground states will be composed of combinations of $|\lambda_2\rangle$, $|\lambda_5\rangle$, and $|\lambda_6\rangle$ on the ladder rungs that minimize the total energy in distinct regions of the parameters. Following this prescription, one can identify four possible ground states. The fully saturated paramagnetic state with the energy per rung $E_P = -2H + 4J$ is given by the eigenvector with all cells in the classical ferromagnetic dimer state $|\lambda_5\rangle$,

$$|P\rangle = \prod_{i=1}^{N} |\lambda_5\rangle_i. \quad (3)$$

The second possible ground state is the classical antiferromagnetic state with an energy per rung $E_{\mathrm{AF}} = -4J$, which is composed of a regular alternation of fully polarized rungs $|\lambda_5\rangle$ and $|\lambda_6\rangle$,

$$|\mathrm{AF}\rangle = \prod_{i=1}^{N/2} |\lambda_5\rangle_{2i-1} \otimes |\lambda_6\rangle_{2i}. \quad (4)$$

The two phases $|P\rangle$ and $|AF\rangle$ have a classical character with no quantum correlation between the electron states. The third ground state is fully quantum with energy per rung $E_Q = (U - \sqrt{\Delta})/2$ and all rungs in the dimer state $|\lambda_2\rangle$,

$$|Q\rangle = \prod_{i=1}^{N} |\lambda_2\rangle_i. \quad (5)$$

This state cannot be written as a direct product of individual states of two mobile electrons on the same rung, which unveils the presence of quantum correlations between them. The fourth ground state with an energy per rung $E_{P,Q} = -H + (U - \sqrt{\Delta})/4$ has a mixed classical-quantum character because it involves a regular alternation of the classical ferromagnetic dimer state $|\lambda_5\rangle$ with the quantum antiferromagnetic dimer state $|\lambda_2\rangle$,

$$|PQ\rangle = \prod_{i=1}^{N/2} |\lambda_5\rangle_{2i-1} \otimes |\lambda_2\rangle_{2i}. \quad (6)$$

The full ground-state phase diagram can be obtained by searching for the lowest-energy state among the four aforementioned eigenstates. All phase boundaries can be analytically obtained from a comparison of the corresponding eigenenergies. In Fig. 2 we plot a set of phase diagrams on the t/J-H/J plane for a few representative values of the Coulomb term. In the absence of Coulomb interaction $U = 0$ all phase boundaries are straight linear lines as shown in Fig. 2(a). At sufficiently low fields, the system undergoes a discontinuous phase transition between the classical antiferromagnetic state AF and the quantum dimer state Q at $t/J = 2$. These two ground states are replaced with the mixed classical-quantum phase PQ at moderate magnetic fields. Finally, the classical saturated paramagnetic phase P appears at strong enough magnetic fields.

The repulsive Coulomb term $U > 0$ leads to a suppression of the parameter regions corresponding to both quantum ground states Q and PQ [see Fig. 2(b)]. The phase boundary between the classical antiferromagnetic state AF and the quantum dimer state Q is, for instance, displaced to larger values of the hopping amplitude $t/J = \sqrt{U/J + 4}$. Similarly, the phase boundaries between the classical ground states (P and AF) and the mixed classical-quantum phase PQ become nonlinear (curved), which results in a reduction of the field range corresponding to the mixed classical-quantum phase PQ.

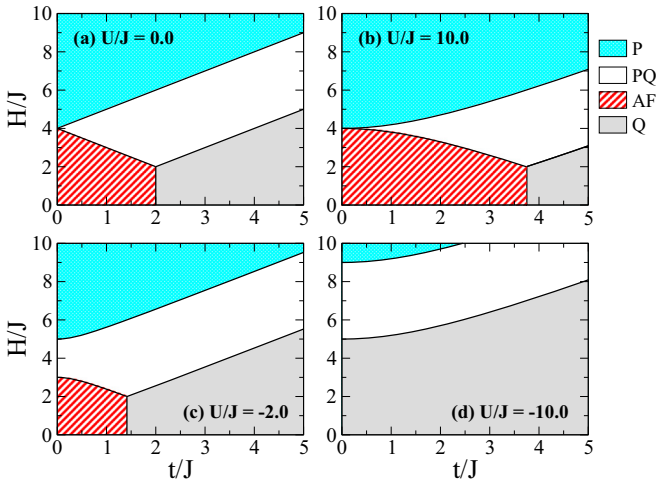

FIG. 2. The ground-state phase diagrams on the t/J-H/J plane for four distinct values of the Coulomb term. The four possible ground states are as follows: the saturated paramagnetic P, the classical antiferromagnetic AF, the fully quantum Q, and the mixed classical-quantum PQ ground state.

For an attractive Coulomb term $U < 0$ there exist two distinct regimes. For weakly attractive electron-electron coupling $|U| < 4J$, the ground-state phase diagram still involves all four available ground states [see Fig. 2(c)], whereas the classical antiferromagnetic phase AF is substantially suppressed. The range of magnetic fields corresponding to the mixed classical-quantum phase PQ emergent in between the classical phases AF and P generally increases, whereas it remains finite even if the hopping term vanishes $t \to 0$. In the strongly attractive regime of the Coulomb interaction $|U| > 4J$, the classical AF phase is fully suppressed, and the system undergoes a sequence of field-induced phase transitions $Q \to PQ \to P$ upon strengthening of the magnetic field regardless of the hopping amplitude [see Fig. 2(d) for an illustration].

III. FERMIONIC QUANTUM ENTANGLEMENT ON THE LADDER RUNGS

Nonseparable physical states imply the presence of intrinsic quantum correlations. This is the case of the dimer eigenstates $|\lambda_i\rangle$ ($i = 1$–4). Several quantities have been introduced in the literature to quantify quantum entanglement, the most natural of them is being von Neumann entropy (also called entropy of formation) [63]. For pure states $|\Psi\rangle$ of a two-parties (AB) system, the degree of quantum entanglement can be directly computed by performing the partial trace of the density matrix $\rho = |\Psi\rangle\langle\Psi|$ over the states of one of the parties. From the reduced density matrix $\rho_A = \mathrm{Tr}_B \rho$, the intrinsic quantum entanglement between the parties can be quantified by computing the entropy of formation $\mathcal{S} = -\sum_j p_j \ln p_j$, where p_j's are the eigenvalues of the reduced density matrix. Note that $\mathcal{S} = 0$ when the state of the parties is a nonentangled direct product of each party state. On the other hand it becomes $\mathcal{S} = \ln n$ for the maximal entanglement of n states.

After performing the partial trace over the states of the dimer sites it can be directly seen that the resulting density matrix for states $|\lambda_3\rangle$ and $|\lambda_4\rangle$ is an even mixture of two states and $\mathcal{S} = \ln 2$. On the other hand, states $|\lambda_1\rangle$ and $|\lambda_2\rangle$ produce a partial density matrix composed on an uneven mixture of four states. A straightforward calculation provides for these states the entropy of formation,

$$\mathcal{S} = \frac{2}{2+2\alpha_2^2}\left[\ln\left(2+2\alpha_2^2\right) + \alpha_2^2 \ln \frac{2+2\alpha_2^2}{\alpha_2^2}\right], \qquad (7)$$

where α_2 is the state coefficient defined in the previous section. It reaches a maximal value of $\mathcal{S} = \ln 4$ for $U = 0$, corresponding to the even mixtures of all four state components with antiparallel spin orientation of the dimer electrons. The minimal value of $\mathcal{S} = \ln 2$ occurs at $|U| \to \infty$ on which the state has the electrons in the same or in distinct sites for strongly attractive or repulsive U, respectively.

At finite temperatures, the dimer state will become a statistical mixture of all possible dimer eigenstates. In this case, there is no simple measure of quantum entanglement of a general bipartite system except for the case in which each party expands a two-dimensional space vector, i.e., for two entangled qubits. In this case, the entanglement of formation is the minimum average entanglement of an ensemble of pure states that represents the density matrix ρ [64,65]. A closely related quantifier is the quantum concurrence that is a monotonic function of the entropy of formation. The quantum concurrence can be directly extracted from the density matrix of the two qubits. Because the entanglement of formation is a monotonous function of the concurrence, one may directly use the concurrence as a measure of quantum entanglement ranging from 0 (no entanglement) up to 1 (maximum entanglement).

In the present model, each dimer site spans a four-dimensional vector state space with base vectors $|0\rangle$, $|\uparrow\rangle$, $|\downarrow\rangle$, and $|\uparrow\downarrow\rangle$. As such, there is no general prescription to fully evaluate the degree of entanglement within a dimer when it is in a thermal statistical mixture of states. An alternative approach is to evaluate the degree of quantum entanglement in specific sectors of the state vector space [66–68]. For example, the charge degrees of freedom within each dimer site with a fixed spin orientation spans a two-dimensional Hilbert space with basis vectors $|0\rangle$ and $|\uparrow\rangle$. In this sector of the Hilbert space, the dimer behaves effectively as two qubits. Here, we will follow a prescription previously introduced to compute the fermionic concurrence of Hubbard dimers in this sector which captures the intrinsic quantum correlations associated with the charge degrees of freedom [44,66,67]. However, it is important to have in mind that the charge correlations represent only a fraction of the actual quantum entanglement between the two parties. In this subspace, the density matrix written in the basis composed of the dimer states $|0,0\rangle$, $|0,\uparrow\rangle$, $|\uparrow,0\rangle$, and $|\uparrow,\uparrow\rangle$ can be put in the form

$$\rho_{1,2} = \begin{pmatrix} a & 0 & 0 & 0 \\ 0 & x & z & 0 \\ 0 & z^* & y & 0 \\ 0 & 0 & 0 & b \end{pmatrix}, \qquad (8)$$

where the elements represent the expectation values of distinct correlations between the two sites,

$$b = \langle n_{1,\uparrow}, n_{2,\uparrow}\rangle,$$
$$x = \langle n_{1,\uparrow}\rangle - \langle n_{1,\uparrow}, n_{2,\uparrow}\rangle,$$

$$y = \langle n_{2,\uparrow}\rangle - \langle n_{1,\uparrow}, n_{2,\uparrow}\rangle,$$
$$a = \langle (1-n_{1,\uparrow})(1-n_{2,\uparrow})\rangle,$$
$$z = z^* = \langle c^\dagger_{1,\uparrow}, c_{2,\uparrow}\rangle. \quad (9)$$

The concurrence is defined in terms of the spectra of the matrix $\rho_{1,2}\bar{\rho}_{1,2}$ [65], where $\bar{\rho}_{1,2} = \sigma_1^y \otimes \sigma_2^y \rho^*_{1,2} \sigma_1^y \otimes \sigma_2^y$ with σ_i^y as a standard Pauli matrix. Being Λ_i the eigenvalues of $\rho_{1,2}\bar{\rho}_{1,2}$, the quantum concurrence is simply given by $\mathcal{C} = \max[0, \sqrt{\Lambda_1} - \sqrt{\Lambda_2} - \sqrt{\Lambda_3} - \sqrt{\Lambda_4}]$ with Λ_1 being the largest eigenvalue [65]. The resulting expression for such fermionic concurrence can be written as

$$\mathcal{C} = 2\ \max\{0, |\langle c^\dagger_{1,\uparrow} c_{2,\uparrow}\rangle| - \sqrt{\langle n_{1,\uparrow} n_{2,\uparrow}\rangle (1 - 2\langle n_{1,\uparrow}\rangle + \langle n_{1,\uparrow} n_{2,\uparrow}\rangle)}\}. \quad (10)$$

The fermionic concurrence in the up spin subspace is null in the nonseparable eigenstates $|\lambda_3\rangle$ and $|\lambda_4\rangle$. This feature reflects that fact that it only captures a fraction of the underlying quantum correlations. However, the fermionic concurrence becomes nonzero in the other two dimer eigenstates $|\lambda_1\rangle$ and $|\lambda_2\rangle$ for which it acquires the nonzero value $\mathcal{C} = 1/\sqrt{1 + (U/4t)^2}$. In Fig. 3 we compare the entropy of formation and the above fermionic concurrence for the pure entangled state $|\lambda_2\rangle$ as a function of the ratio U/t. Both quantities are maximal at $U = 0$ for which the dimer state is an even superposition of all its four possible states with antiparallel spins. The minimal entanglement of these states takes place in the regime of $|U| \to \infty$ at which two state components are suppressed. This trend is captured by both entanglement quantifiers, although the fermionic concurrence vanishes in this limit because it does not retain information concerning the remaining quantum correlation between the spin degrees of freedom. Considering that the fermionic concurrence can be also computed for the statistically mixed states appearing at finite temperatures, we will discuss its main features under the light of the ground-state phase diagram and the influence of thermal excitations on it.

Accordingly, the two classical ground-states P and AF have $\mathcal{C} = 0$ at zero temperature. The quantum dimer phase Q has the same fermionic quantum concurrence as the eigenstate $|\lambda_2\rangle$, whereas the averaged fermionic concurrence of the mixed classical-quantum ground-state PQ has half of this value. Bearing this in mind, the fermionic quantum concurrence exhibits a discontinuous jump at all phase boundaries. In Fig. 4 we illustrate the dependence of the fermionic concurrence on the hopping amplitude in the low-field and intermediate-field regimes for the same representative values of the Coulomb interaction as previously used in the ground-state phase diagrams. In the low-field regime [Fig. 4(a)] the system exhibits a direct field-induced transition from the classical antiferromagnetic phase AF to the quantum antiferromagnetic phase Q. Notice that maximal fermionic entanglement $\mathcal{C} = 1$ is achieved in the quantum dimer phase Q when the Coulomb term is absent $U = 0$ or, equivalently, in the limit of $t/J \to \infty$. Note furthermore that the quantum dimer phase Q becomes the only possible ground state at low enough magnetic fields for strong attractive Coulomb terms $U/J < -4$. In the regime of

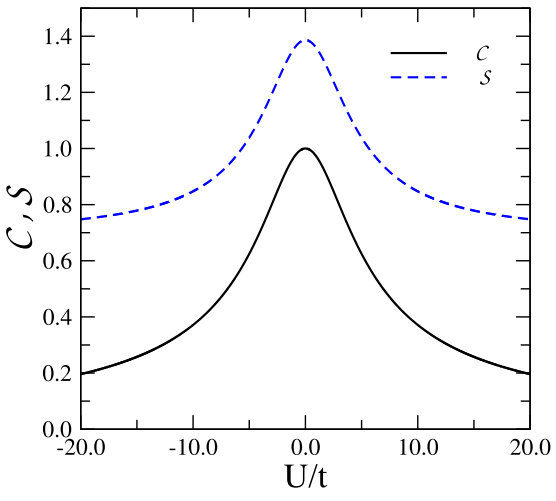

FIG. 3. The entropy of formation $\mathcal{S}$ and fermionic concurrence $\mathcal{C}$ as a function of U/t for the dimer eigenstate $|\lambda_2\rangle$. Both entanglement measures have similar trends being maximal at $U = 0$ and decaying as $|U|$ increases. Note that the fermionic concurrence vanishes when $|U| \to \infty$ whereas the entropy of formation remains finite. This behavior signals that the asymptotic state presents quantum correlations in other degrees of freedom besides the charge ones probed by $\mathcal{C}$.

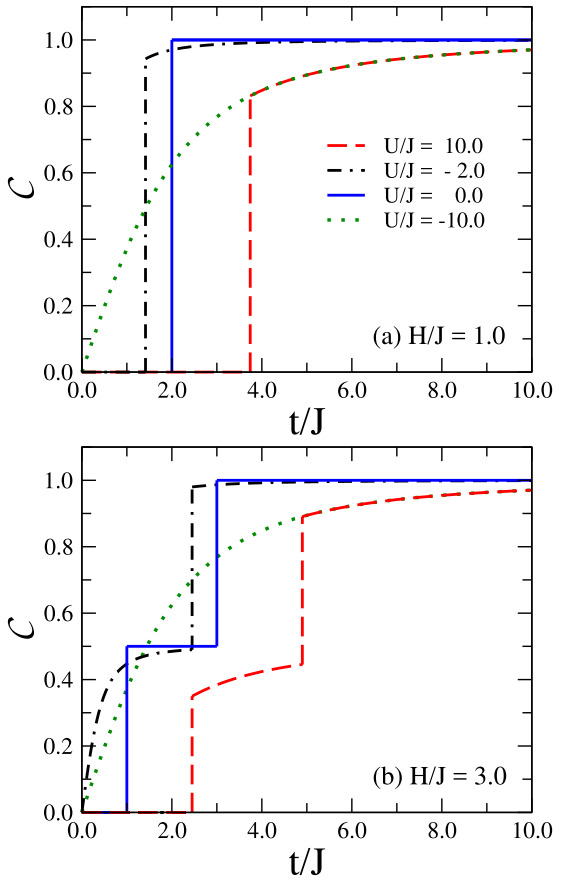

FIG. 4. The zero-temperature fermionic concurrence at the dimer rungs as a function of the normalized hopping amplitude t/J for two representative values of the magnetic field and four distinct values of the Coulomb term U/J. The discontinuous jumps signal the field-driven phase transitions. A full entanglement is achieved in the quantum antiferromagnetic phase Q in the limit $t/|U| \to \infty$.

intermediate magnetic fields [Fig. 4(b)], the two discontinuous jumps in the fermionic concurrence signal the field-driven phase transitions $AF \rightarrow PQ$ and $PQ \rightarrow Q$, respectively. The complete suppression of the classical antiferromagnetic phase AF for strongly attractive Coulomb interactions either leads to a single discontinuous jump in the fermionic concurrence closely connected with the field-driven phase transition $PQ \rightarrow Q$ [see the curve $U/J = -2$ in Fig. 4(b)] or to a monotonous rise of the fermionic concurrence within the quantum dimer ground state Q [see the curve $U/J = -10$ in Fig. 4(b)].

In order to investigate how thermal fluctuations affect the fermionic concurrence on the present Ising-Hubbard ladder, we have computed the partition function using the standard transfer-matrix formalism. The partition function can be written as $\mathcal{Z} = \mathrm{Tr}\,\Lambda^N$, where $\Lambda = e^{-\beta H_{i,i+1}}$ with $H_{i,i+1}$ being the symmetrized cell Hamiltonian connecting the ladder rungs i and $i+1$ and $\beta = 1/k_B T$. In the basis of the dimer eigenstates, the elements of the transfer matrix are given by

$$\langle \lambda_i | \Lambda | \lambda_j \rangle = e^{-\beta[J S_i^z S_j^z + (E_i + E_j)/2]}, \tag{11}$$

where S_i^z is the z component of the total spin of the ith dimer eigenstate. The full transfer matrix has the following explicit form:

$$\Lambda = \begin{pmatrix} x^2 r^{-2} & x^2 & x^3 r^{-1} & xr^{-1} & xzr^{-1} & xz^{-1}r^{-1} \\ x^2 & x^2 r^2 & x^3 r & xr & xzr & xrz^{-1} \\ x^3 r^{-1} & x^3 r & x^4 & x^2 & x^2 z & x^2 z^{-1} \\ xr^{-1} & xr & x^2 & 1 & z & z^{-1} \\ xzr^{-1} & xzr & x^2 z & z & yz^2 & y^{-1} \\ xz^{-1}r^{-1} & xrz^{-1} & x^2 z^{-1} & z^{-1} & y^{-1} & yz^{-2} \end{pmatrix}, \tag{12}$$

where

$$x = e^{-\beta U/4}, \tag{13}$$

$$r = e^{\beta\sqrt{\Delta}/4}, \tag{14}$$

$$z = e^{\beta H}, \tag{15}$$

$$y = e^{-4\beta J}. \tag{16}$$

The above transfer matrix can be diagonalized with a high numerical accuracy in order to get the partition function $\mathcal{Z} = \mathrm{Tr}\,\lambda^N = \lambda^N$, which is expressed in terms of the largest eigenvalue λ of the transfer-matrix (12). Alternatively, the eigenvalues and eigenvectors can be obtained from the algebraic solution of a fourth order polynomial equation after noting that the above transfer matrix has two null eigenvalues. However, the resulting expressions are quite cumbersome and do not unveil any relevant aspect of the system's thermodynamics. All thermodynamic averages can be directly computed from the knowledge of the transfer-matrix eigenvalues and eigenvectors. In the following, we will focus in the resulting temperature dependence of the fermionic concurrence.

In Fig. 5 we plot the fermionic concurrence as a function of temperature for the particular case without the Coulomb interaction [Fig. 5(a)] and the particular case with a strong repulsive Coulomb interaction [Fig. 5(b)]. Four distinct sets of physical parameters were used to probe all possible ground states. Similar trends are obtained in both noninteracting and strongly repulsive cases. Whenever the ground state has a finite fermionic entanglement (PQ and Q phases), thermal fluctuations continuously degrade the quantum correlations until the fermionic concurrence finally vanishes above a certain threshold temperature. However, thermal fluctuations play quite distinct roles above the classical ground states. Although the fermionic concurrence remains zero for all temperatures above the classical antiferromagnetic phase AF, some degree of quantum entanglement can be thermally induced above the saturated paramagnetic phase P.

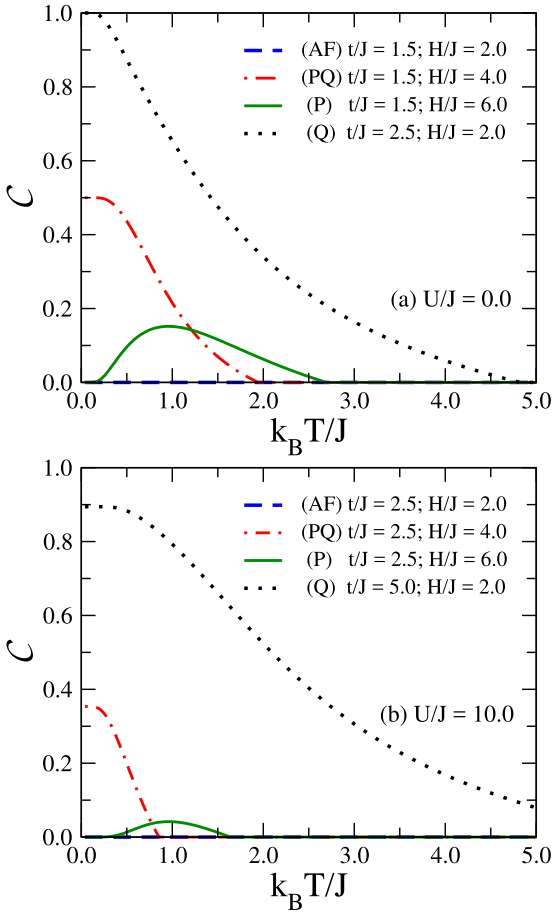

FIG. 5. Temperature dependence of the fermionic concurrence for a few representative values of the magnetic field, the hopping amplitude, and two selected values of the Coulomb term: (a) $U/J = 0$; (b) $U/J = 10$. Thermal fluctuations may induce emergence of fermionic concurrence above the classical saturated paramagnetic phase P but not above the classical antiferromagnetic phase AF.

The aforedescribed thermally induced entanglement can also be clearly seen from the field dependence of the fermionic concurrence shown in Fig. 6 for a few different temperatures. For illustration, the fermionic concurrence is only plotted for the special case without the Coulomb interaction, but the main features remain the same also for finite values of the Coulomb term. In Fig. 6(a) we have used a set of parameters for which the classical antiferromagnetic phase AF constitutes the zero-field ground state. It is noteworthy that the lower threshold temperature at which the fermionic concurrence starts to develop is displaced to larger field values as the temperature is raised from zero. This means that no fermionic entanglement

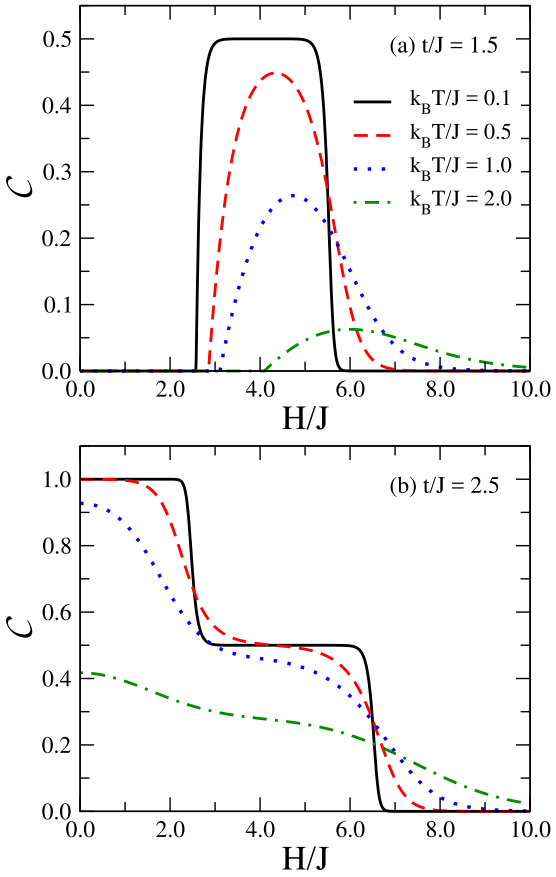

FIG. 6. The fermionic concurrence versus the magnetic field for the particular case with zero Coulomb term $U = 0$ and two representative values of the hopping amplitude, which drive the zero-field ground state of the investigated system either to: (a) the classical antiferromagnetic phase AF or (b) the quantum antiferromagnetic phase Q. Both threshold fields shift towards higher values with increasing temperatures, which means that thermal fluctuations induce the fermionic concurrence above the saturated paramagnetic phase P.

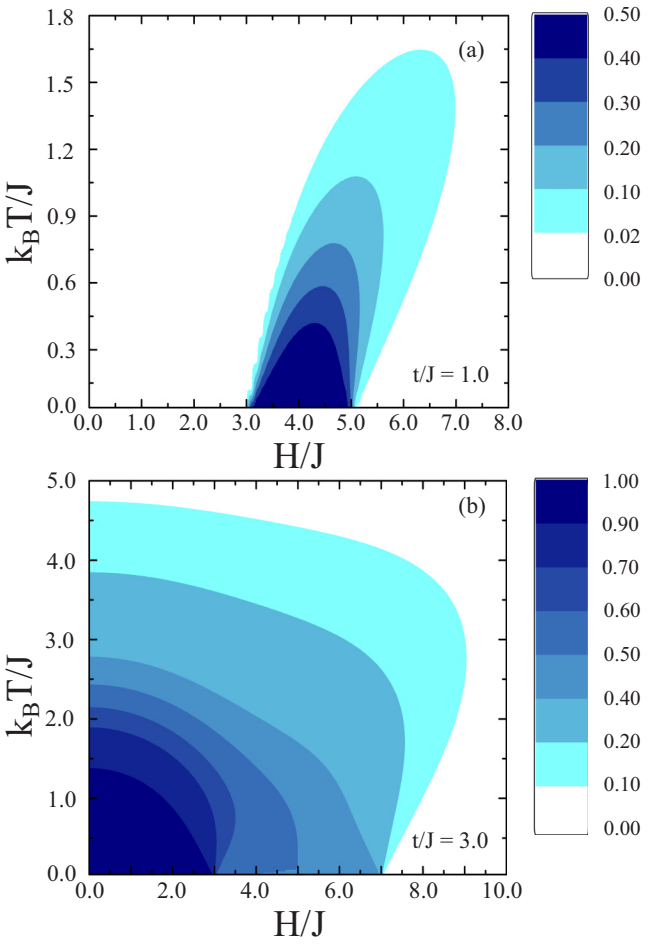

FIG. 7. Density plots of the fermionic concurrence on the k_BT/J-H/J plane for the particular case without the Coulomb term $U = 0$ and two distinct values of the hopping amplitude leading to different zero-field ground states. Note the re-entrance of the region with finite fermionic concurrence. The higher temperatures at which fermionic entanglement can still be achieved are found for magnetic fields strong enough to drive the system to the classical saturated paramagnetic ground state.

can be generated at finite temperatures above the classical antiferromagnetic ground state AF. The second threshold temperature at which the fermionic concurrence returns to zero is also displaced to larger fields. This result is taken to mean that thermal fluctuations promote the emergence of fermionic concurrence above the saturated paramagnetic phase P although the maximum entanglement that can be produced by tuning the magnetic field decreases as the temperature increases.

A full understanding of the field and temperature dependences of the fermionic concurrence can be obtained from the density plots displayed in Fig. 7. At low hopping amplitudes [see Fig. 7(a)], the low-field ground state is the classical antiferromagnetic phase AF with zero fermionic concurrence. The re-entrant behavior of the concurrence is clearly signaled by the bending of the region with finite concurrence towards larger fields. For high hopping amplitudes [see Fig. 7(b)], the low-field ground state is the quantum antiferromagnetic phase Q with maximal concurrence. In this regime, the thermally induced entanglement is also reflected by the re-entrant behavior of the quantum concurrence. It is interesting to note that the largest temperatures at which some degree of quantum fermionic entanglement can be generated are found at magnetic fields corresponding to the disentangled saturated paramagnetic phase P at low enough temperatures.

The physical mechanism leading to the re-entrant character of the fermionic entanglement is the thermal excitation from a nonentangled ground state to an entangled excited state. In general, thermal fluctuations degrade quantum entanglement due to the incoherent coupling with degrees of freedom of the heat bath. However, when the energy gap between the nonentangled ground state and an excited entangled state is small (usually in the vicinity of ground-state phase transitions), the system populates the entangled state at temperatures that are not sufficient to degrade its quantum correlations. Under this condition, quantum entanglement appears at finite temperatures above a nonentangled ground state. A similar trend also occurs in other quantum spin models as, for example, in antiferromagnetic Heisenberg chains for magnetic fields slightly above the saturation value [1].

IV. SUMMARY AND CONCLUSIONS

To summarize, we have introduced a new exactly solvable Ising-Hubbard ladder model. The ladder rungs were considered to be composed of the Hubbard dimers at half-filling on each rung, which take into account a quantum-mechanical intrarung hopping process of the mobile electrons as well as the on-site Coulomb interaction. The interaction between the electrons from neighboring rungs was assumed to be Ising-like. The model was exactly solved using the exact diagonalization and transfer-matrix technique, whereas our attention was particularly focused on the most interesting case with the antiferromagnetic Ising coupling. Both cases of attractive and repulsive Hubbard interactions were considered.

It has been shown that the investigated model exhibits four possible ground states. Two of them are classical: the saturated paramagnetic phase P and the classical antiferromagnetic phase AF. The other two ground states are of quantum nature. There exists a fully quantum dimer ground-state Q with all Hubbard dimers in the same quantum entangled state. The fourth ground-state PQ has a mixed classical-quantum nature because of a regular alternation of the Hubbard dimers in the disentangled and entangled states. It has been demonstrated that the classical antiferromagnetic phase AF is fully suppressed when the Hubbard interaction becomes strongly attractive.

The degree of quantum entanglement between the pair of electrons in a given ladder rung was evaluated by computing the fermionic concurrence in the subspace of up spins. It has been convincingly evidenced that the fully quantum antiferromagnetic phase Q is maximally entangled for the special case with zero Coulomb term $U = 0$. The fermionic concurrence continuously decreases as the Coulomb term $|U|$ strengthens, whereas it approaches zero in the atomic limit $U \to \infty$. It has been also shown that thermal fluctuations generally degrade the degree of quantum entanglement especially when the ground state is of a quantum nature. The electrons remain disentangled at any temperature when the ground state is formed by the classical antiferromagnetic phase AF. By contrast, thermal fluctuations may induce a finite degree of quantum entanglement above the classical saturated paramagnetic state. This striking finding is evidenced by a re-entrant character of the fermionic concurrence as a function of temperature when the magnetic field is chosen slightly above its saturation value. Some degree of quantum fermionic entanglement can be thus achieved at relatively high temperatures when a sufficiently strong magnetic field drives the system towards the classical paramagnetic phase. Under this condition, quantum information processing schemes can be implemented at moderated temperatures even when the system has a factorizable ground state [69].

It is worth emphasizing that the quantum concurrence in a Bose-Hubbard chain has been experimentally probed between ultracold atoms trapped in optical lattices through measures of transverse spin correlations [24]. It is our hope that the here obtained results are of general validity and provide insight for more realistic fermionic models. We believe that the phenomenology reported here will remain valid when the electron hopping is also allowed between neighboring dimers, at least, in the regime of weak inter-rung hopping amplitudes for which the Mott insulator regime is developed. However, the corresponding strongly correlated itinerant electron model is not exactly solvable, and numerical calculations based on the density matrix renormalization group technique [70] or exact diagonalization of finite chains [68] will be required to address this question. We hope that the present paper will stimulate future efforts along this line.

ACKNOWLEDGMENTS

This work was supported by CAPES (Coordenação de Aperfeiçoamento de Pessoal de Nível Superior), CNPq (Conselho Nacional de Desenvolvimento Científico e Tecnológico), and FAPEAL (Fundação de Apoio à Pesquisa do Estado de Alagoas). J.S. acknowledges financial support by a grant from The Ministry of Education, Science, Research and Sport of the Slovak Republic under Contract No. VEGA 1/0043/16 and by a grant from the Slovak Research and Development Agency under Contract No. APVV-0097-12.

[1] M. C. Arnesen, S. Bose, and V. Vedral, Phys. Rev. Lett. **87**, 017901 (2001).
[2] S. Bose, Contemp. Phys. **48**, 13 (2007).
[3] M. B. Plenio and F. L. Semiao, New J. Phys. **7**, 73 (2005).
[4] M. B. Plenio and S. Virmani, Phys. Rev. Lett. **99**, 120504 (2007).
[5] M. Popp, F. Verstraete, M. A. Martin-Delgado, and I. Cirac, Appl. Phys. B **82**, 225 (2006).
[6] L. Amico, A. Osterloh, F. Plastina, R. Fazio, and G. M. Palma, Phys. Rev. A **69**, 022304 (2004).
[7] T. J. G. Apollaro and F. Plastina, Phys. Rev. A **74**, 062316 (2006).
[8] F. Plastina and T. J. G. Apollaro, Phys. Rev. Lett. **99**, 177210 (2007).
[9] M. J. Hartmann, M. E. Reuter, and M. B. Plenio, New J. Phys. **8**, 94 (2006).
[10] L. C. Venuti, S. M. Giampaolo, F. Illuminati, and P. Zanardi, Phys. Rev. A **76**, 052328 (2007).
[11] T. S. Cubitt and J. I. Cirac, Phys. Rev. Lett. **100**, 180406 (2008).
[12] G. Gualdi, S. M. Giampaolo, and F. Illuminati, Phys. Rev. Lett. **106**, 050501 (2011).
[13] M. P. Estarellas, I. D'Amico, and T. P. Spiller, Phys. Rev. A **95**, 042335 (2017).
[14] E. Dagotto and T. M. Rice, Science **271**, 618 (1996).
[15] M. Uehara, T. Nagata, J. Akimitsu, H. Takahashi, N. Môri, and K. Kinoshita, J. Phys. Soc. Jpn. **65**, 2764 (1996).
[16] T. Hong, Y. H. Kim, C. Hotta, Y. Takano, G. Tremelling, M. M. Turnbull, C. P. Landee, H.-J. Kang, N. B. Christensen, K. Lefmann, K. P. Schmidt, G. S. Uhrig, and C. Broholm, Phys. Rev. Lett. **105**, 137207 (2010).
[17] M. Klanjsek, H. Mayaffre, C. Berthier, M. Horvatic, B. Chiari, O. Piovesana, P. Bouillot, C. Kollath, E. Orignac, R. Citro, and T. Giamarchi, Phys. Rev. Lett. **101**, 137207 (2008).

[18] K. Ninios, T. Hong, T. Manabe, C. Hotta, S. N. Herringer, M. M. Turnbull, C. P. Landee, Y. Takano, and H. B. Chan, Phys. Rev. Lett. **108**, 097201 (2012).

[19] D. G. Angelakis, M. F. Santos, and S. Bose, Phys. Rev. A **76**, 031805(R) (2007).

[20] G. M. A. Almeida, F. Ciccarello, T. J. G. Apollaro, and A. M. C. Souza, Phys. Rev. A **93**, 032310 (2016).

[21] P. Cappellaro, C. Ramanathan, and D. G. Cory, Phys. Rev. A **76**, 032317 (2007).

[22] G. A. Alvarez and D. Suter, Phys. Rev. Lett. **104**, 230403 (2010).

[23] R. Islam, R. Ma, P. M. Preiss, M. E. Tai, A. Lukin, M. Rispoli, and M. Greiner, Nature (London) **528**, 77 (2015).

[24] T. Fukuhara, S. Hild, J. Zeiher, P. Schauß, I. Bloch, M. Endres, and C. Gross, Phys. Rev. Lett. **115**, 035302 (2015).

[25] M. Cao and S. Q. Zhu, Phys. Rev. A **71**, 034311 (2005).

[26] R. Xin, Z. Song, and C. P. Sun, Phys. Lett. A **342**, 30 (2005).

[27] G. L. Kamta and A. F. Starace, Phys. Rev. Lett. **88**, 107901 (2002).

[28] X. G. Wang, Phys. Rev. A **66**, 044305 (2002).

[29] O. Osenda, Z. Huang, and S. Kais, Phys. Rev. A **67**, 062321 (2003).

[30] L. Zhou, H. S. Song, Y. Q. Guo, and C. Li, Phys. Rev. A **68**, 024301 (2003).

[31] G. F. Zhang and S. S. Li, Phys. Rev. A **72**, 034302 (2005).

[32] A. Tribedi and I. Bose, Phys. Rev. A **79**, 012331 (2009).

[33] S.-J. Gu, H.-Q. Lin, and Y.-Q. Li, Phys. Rev. A **68**, 042330 (2003).

[34] B.-Q. Jin and V. E. Korepin, Phys. Rev. A **69**, 062314 (2004).

[35] L. F. Santos, G. Rigolin, and C. O. Escobar, Phys. Rev. A **69**, 042304 (2004).

[36] H. A. Zad and N. Ananikian, J. Phys.: Condens. Matter **29**, 455402 (2017).

[37] J. Strečka and J. Pavlicko, Acta. Phys. Pol. A **132**, 167 (2017).

[38] B. Lisnyi and J. Strečka, Physica A **462**, 104 (2016).

[39] R. C. Alecio, M. L. Lyra, and J. Strečka, J. Magn. Magn. Matter. **417**, 294 (2016).

[40] O. Rojas, J. Strečka, and S. M. de Souza, Solid State Commun. **246**, 68 (2016).

[41] J. Strečka, R. C. Alecio, M. L. Lyra, and O. Rojas, J. Magn. Magn. Matter. **409**, 124 (2016).

[42] V. V. Hovhannisyan, J. Strečka, and N. S. Ananikian, J. Phys.: Condens. Matter **28**, 085401 (2016).

[43] Y.-D. Zheng, Z. Mao, and B. Zhou, Acta. Phys. Sin. **66**, 230304 (2017).

[44] J. Torrico, M. Rojas, M. S. S. Pereira, J. Strečka, and M. L. Lyra, Phys. Rev. B **93**, 014428 (2016).

[45] M. Rojas, S. M. de Souza, and O. Rojas, Phys. Rev. A **89**, 032336 (2014).

[46] J. Torrico, M. Rojas, S. M. de Souza, O. Rojas, and N. S. Ananikian, Europhys. Lett. **108**, 50007 (2014).

[47] J. Strečka, O. Rojas, T. Verkholyak, and M. L. Lyra, Phys. Rev. E **89**, 022143 (2014).

[48] H. G. Paulinelli, S. M. de Souza, and O. Rojas, J. Phys.: Condens. Matter **25**, 306003 (2013).

[49] O. Rojas, M. Rojas, N. S. Ananikian, and S. M. de Souza, Phys. Rev. A **86**, 042330 (2012).

[50] N. S. Ananikian, L. N. Ananikyan, L. A. Chakhmakhchyan, and O. Rojas, J. Phys.: Condens. Matter **24**, 256001 (2012).

[51] M. S. S. Pereira, F. A. B. F. de Moura, and M. L. Lyra, Phys. Rev. B **77**, 024402 (2008).

[52] M. S. S. Pereira, F. A. B. F. de Moura, and M. L. Lyra, Phys. Rev. B **79**, 054427 (2009).

[53] M. Nalbandyan, H. Lazaryan, O. Rojas, S. M. Souza, and N. Ananikian, J. Phys. Soc. Jpn. **83**, 074001 (2014).

[54] H. Lazaryan, M. Nalbandyan, and N. Ananikian, Int. J. Mod. Phys. B **30**, 1650135 (2016).

[55] J. Torrico, M. S. S. Pereira, J. Strečka, and M. L. Lyra, Acta Phys. Pol. A **132**, 140 (2017).

[56] R. C. P. Carvalho, M. S. S. Pereira, I. N. de Oliveira, J. Strečka, and M. L. Lyra, J. Phys.: Condens. Matt. **29**, 365801 (2017).

[57] A. Moreo and D. J. Scalapino, Phys. Rev. Lett. **98**, 216402 (2007).

[58] L. Hackermuller, U. Schneider, M. Moreno-Cardoner, T. Kitagawa, T. Best, S. Will, E. Demler, E. Altman, I. Bloch, and B. Paredes, Science **327**, 1621 (2010).

[59] D. Allen, F. H. L. Essler, and A. A. Nersesyan, Phys. Rev. B **61**, 8871 (2000).

[60] G.-H. Liu, H.-L. Wang, and G.-S. Tian, Phys. Rev. B **77**, 214418 (2008).

[61] L. J. de Jongh and A. R. Miedema, Adv. Phys. **23**, 1 (1974).

[62] W. P. Wolf, Braz. J. Phys. **30**, 794 (2000).

[63] M. Keyl, Phys. Rep. **369**, 431 (2002).

[64] S. Hill and W. K. Wootters, Phys. Rev. Lett. **78**, 5022 (1997).

[65] W. K. Wootters, Phys. Rev. Lett. **80**, 2245 (1998).

[66] S. J. Gu, S. S. Deng, Y. Q. Li, and H. Q. Lin, Phys. Rev. Lett. **93**, 086402 (2004).

[67] S. S. Deng and S. J. Gu, Chin. Phys. Lett. **22**, 804 (2005).

[68] A. Rycerz, New J. Phys. **19**, 053025 (2017).

[69] T. Chanda, T. Das, D. Sadhukhan, A. K. Pal, A. Sen(De), and U. Sen, Phys. Rev. A **97**, 012316 (2018).

[70] W. L. Chan and S. J. Gu, J. Phys.: Condens. Matter **20**, 345217 (2008).